



EDTA-Functionalized Magnetic Graphene Oxide/Polyacrylamide Grafted Carboxymethyl Cellulose Hydrogel for Removal of Pb^{2+} from Aqueous Solution

Sawsan Dacropy¹ · Kholod H. Kamal² · Samir Kamel¹

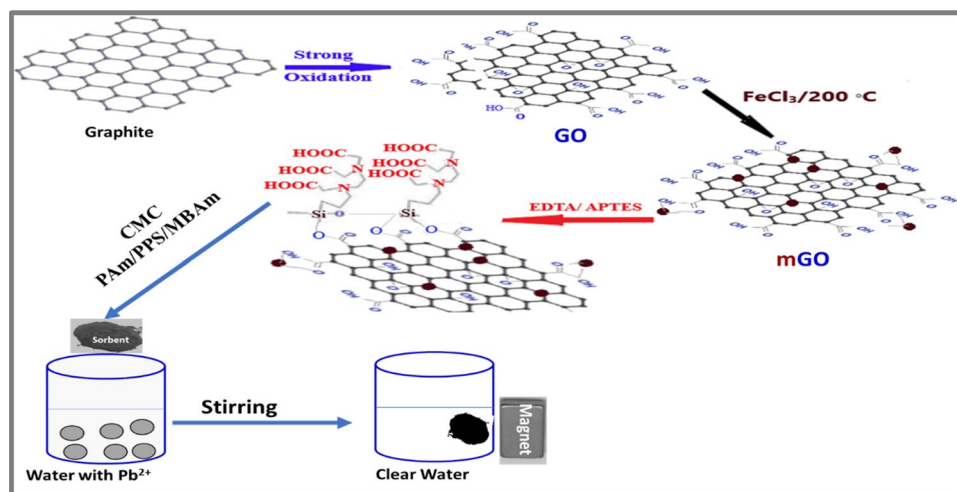
Accepted: 7 October 2021 / Published online: 26 October 2021

© The Author(s), under exclusive licence to Springer Science+Business Media, LLC, part of Springer Nature 2021

Abstract

A promising sorbent was prepared by a combination of different eco-friendly functional groups such as ethylenediaminetetraacetic acid with 3-aminopropyltriethoxysilane (EDTA/Si) and polyacrylamide grafted carboxymethyl cellulose (AmCMC) with magnetic graphene oxide (mGO) and N,N-Methylene bis-acrylamide as a crosslinker for efficient removal of lead ions (Pb^{2+}) from aqueous solutions. The prepared sorbent was characterized by X-ray diffraction (XRD), infrared spectroscopy (FTIR), thermal gravimetric analysis (TGA), the scanning electron microscope (SEM), Vibrating sample magnetometer (VSM), and Zeta-potential measurements. The oxidation of graphite was confirmed by XRD and transmission electron microscope (TEM). The adsorption conditions such as contact time, pH, sorbent dosage, and initial Pb^{2+} concentrations were investigated to optimize the adsorption efficiency of the prepared sorbent. EDTA/Si/mGO/AmCMC was found to be an ideal sorbent for Pb^{2+} removal with a higher adsorption capacity due to the successive link of chelating groups onto AmCMC. From the data, at $\text{pH} = 5.3$ after 120 min, EDTA/Si/mGO/AmCMC has high removal efficiency of Pb^{2+} (92%) compared with AmCMC (46%). For deep information, Kinetic and isotherm models were applied for the adsorption process. From the data, the harmony of data fitting with the pseudo-second-order kinetic model and the Langmuir isotherm model. According to the Langmuir adsorption isotherms, the maximum adsorption capacity of 0.15 g EDTA/Si/mGO/AmCMC at $\text{pH} = 5.3$ after 120 min is 86 mg/g.

Graphic Abstract



Keywords Cellulose · Graphene oxide · EDTA · Magnetite · Pb^{2+} adsorption · Kinetic and isotherm study

Extended author information available on the last page of the article

Highlights

1. EDTA functionalized mGO were synthesized.
2. Grafted CMC hydrogel embedded with EDTA functionalized mGO was prepared.
3. The prepared adsorbent has high adsorption capacity for Pb^{+2} .
4. The adsorption process fitted with pseudo-second-order and Langmuir models.

Introduction

Water shortage is a great challenge that faces the entire world, specifically in the Middle East. At the same time, the drinking water is a major burden in many countries due to scarcity of water as a result of an absence of water sources and/or due to water pollution. So, discovering new resources of water became an essential issue [1, 2]. Consequently, the researchers try to find new approaches to preserve water from pollution, treat or reuse water, as well as extract groundwater [3–6]. The entire removal of pollutants in the resources of water protects the environment as well as stops the transfer of toxic contaminant in food chains. One of the most common pollutants in water are heavy metals which adversely affect the environmental and human health [7]. Many conventional approaches have been employed to remove heavy metals from water such as chemical precipitation, ion-exchange, reverse osmosis, filtration, membrane technologies, and electrochemical methods [8, 9]. However, the sorption process is one of the most productive, simply flexible, and most cost-effective methods [10]. Several sorbents have been studied for metal removals like inorganic materials, activated carbon, zeolite, and resins but these sorbents have been suffering from either low efficiencies or low adsorption capacities [11–14]. Therefore, in recent years a great effort to prepare new sorbents and develop new techniques has been made. New as well as eco-friendly materials and composites were used in the sorption processes such as cellulose, carrageenan, and hydrogels [15, 16]. Hydrogels are 3D cross linked polymers that can absorb a lot of water into their structure [17]. So, it looks like a promising heavy metal removal. Various natural biopolymers can be used to prepare hydrogel such as chitosan, cellulose and carboxymethyl cellulose [18, 19]. Cellulose is a green natural, non-toxic, biodegradable, and biocompatible polymer that has been reported to be a promising material used in a vast number of applications [4, 5, 20, 21]. Its characteristics can be altered by physical and/or chemical modifications

depending on the end product needed [22, 23]. The most widespread derivative of cellulose is carboxymethylcellulose (CMC). It is a water-soluble anionic polysaccharide that has great importance in the industry and our everyday life [24, 25]. It is commonly utilized in many fields of industrial applications such as cosmetics, pharmaceuticals, and packaging [22, 26].

Among other eco-sorbents, carbon-based nanomaterials have been studied as superior sorbents for the removal of metal pollutants from aqueous solutions with high capacity and selectivity [27]. Nanomaterials have great impact in wastewater treatment applications in the recent years due to their remarkable properties. Graphene oxide (GO) is one of these materials that holds promising properties due to its unique structure [28]. It is composed of a single layer of graphene bound to oxygen in the form of carboxyl, hydroxyl, or epoxy groups. Due to its mechanical, electronic, optical, and thermal properties, GO has a major role in many applications such as energy storage devices, flexible electronics, sensors, and solar cells [18, 29].

In recent years, magnetic and surface-modified magnetic composites have been developed and used for metal removal due to their rapid separation from an aqueous solution and led to increase adsorption capacity and chemical stability of adsorbents [30, 31]. The introduction of the huge amount of OH groups onto the magnetic surface during the preparation process makes magnetite become hydrophilic in an aqueous solution. On the other hand, the chelating characteristic of ethylenediaminetetraacetic acid (EDTA) may be used to synthesize EDTA-functionalized magnetic particles [32]. When magnetic particles reacted with EDTA and aminopropyl triethoxysilane, the hydrolysis of the trialkoxy groups generates Si–OH groups that react with Fe–OH of magnetic particles surface. Accordingly, EDTA can link to the iron oxide surface through Si–O–Fe bonds and chelating groups are introduced onto the magnetic surface [32, 33].

Accordingly, this contribution presents the synthesis of a new sorbent by embedded EDTA modified magnetic graphene oxide onto polyacrylamide grafted CMC with N,N-Methylene bis-acrylamide as a crosslinker. The prepared sorbent was characterized by several tools such as XRD, FTIR, SEM, TEM, TGA, VSM, and Zeta-potential. The efficiency of the prepared sorbent has been investigated for the removal of Pb^{2+} . The changing of the adsorption conditions was studied to investigate the isotherms and kinetics of the adsorption process.

Materials and Methods

Materials

Sodium carboxymethyl cellulose (CMC) medium viscosity, 98.5% with DS = 0.70–0.85 was purchased from Fluka. Sulfuric Acid (99.9%) was acquired from Sigma Aldrich, USA. Graphite powder (99.9%) was received from Fisher Scientific, UK. Potassium permanganate (KMnO_4), (> 99%), and hydrogen peroxide were provided from Bio Basic Canada Inc. and Carl Roth GmbH, respectively. Potassium persulfate (PPS), and ferric chloride (FeCl_3), 3-aminopropyltriethoxysilane (APTES) were purchased from Fluka. Polyacrylamide, N,N-Methylene bis-acrylamide (MBAm) were purchased from Merck. Potassium Permanganate, Sodium Nitrate (NaNO_3), (99.99%) was bought from Sd Fine-CHE Mlimited, India. Lead nitrate salt [$\text{Pb}(\text{NO}_3)_2$], (99%) was brought from Loba Chemie Co., India. All chemicals were used as received without further treatment.

Methods

Preparation of Graphene Oxide (GO)

To a solution of 7.5 g sodium nitrate in 230 mL of concentrated sulfuric acid, 15 g of graphite powder was added with decreasing the temperature to 0 °C. This following by slow addition of 45 g of potassium permanganate with raise in the temperature to the ambient value. After 3 h under vigorous stirring, 700 mL of distilled water was added and the temperature was kept at 98 °C. After 20 min of stirring, hot distilled water (2100 mL) was added followed by 150 mL of hydrogen peroxide to avoid effervescence. The suspended graphite oxide was sonicated for 30 min, filtered out, and washed with hot distilled water until pH ~ 7, collected (the brown paste), and dried under vacuum at 60 °C [29, 34].

Preparation of Magnetic Graphene Oxide (GO/Fe3O4) (mGO)

The solvothermal method was used to load the magnetite onto GO. A mixture of GO (1 g) and ethylene glycol (150 mL) was ultrasonicated for 2.5 h and the temperature was settled up to 30 °C. $\text{FeCl}_3 \cdot 6\text{H}_2\text{O}$ (3.2 g) and sodium acetate (6.0 g) were added to the mixture and stirred for 40 min. The mixture was heated to 200 °C and for 8 h in a Teflon-lined stainless-steel autoclave. The precipitate (mGO) was magnetically separated, washed with distilled water and ethanol, dried in a vacuum oven at 50 °C for 2 days.

Modification of mGO by EDTA and APTES

In a round bottom flask, 1 g mGO was dispersed in 40 mL of toluene followed by the addition of 0.9 mL of 3-aminopropyltriethoxysilane (APTES). The mixture was refluxed in a water bath at 90 °C for 2 h with rotated at 30 rpm (revolutions/minute). 500 mg EDTA and 50 mL pyridine were added after cooling the mixture to room temperature. Again, the mixture was refluxed in a water bath for 2 h with rotation at 30 rpm. To adjust the pH, 100 mL of sodium bicarbonate (0.5 M) was added after cooling the mixture to room temperature. The supernatant was decanted and the particles were recovered by using a magnet (EDTA/Si/mGO). The EDTA/Si/mGO particles were rinsed twice by deionized water and retaining the particles with the magnet. The same was performed twice with ethanol and then diethyl ether and dried the particles at room temperature for 24 h, and stored in desiccators [33].

Preparation of Sorbent

The loading of EDTA/Si/mGO onto polyacrylamide grafted carboxymethyl cellulose (AmCMC) was performed using a surface deposition-crosslinking method. In a typical preparation, a calculated amount of potassium persulfate (KPS) (0.22 mM \approx 0.06 g/1 g CMC) was added to an aqueous solution of CMC and heated at 60 °C. After 15 min 2 g PAm and MBAm (0.8 mM, 0.12 g/1 g CMC) were added and the mixture was kept at 80 °C for 2 h with stirring. The calculated amount of EDTA/Si/mGO (0.2 g/1 g CMC) was added before the addition of the crosslinker. The mixture was frozen in a deep-freezer followed by the freeze-drying process (ALPHA 1–2/LD PLUS, Martin Christ, Germany).

Characterization

FT-IR spectra were recorded in the range of 400–4000 cm^{-1} on (Shimadzu 8400S) FT-IR Spectrophotometer. The XRD patterns were investigated on a Diano X-ray diffractometer using $\text{CoK}\alpha$ radiation source energized at 45 kV and a Philips X-ray diffractometer (PW 1930 generator, PW 1820 goniometer) with CuK radiation source ($\lambda = 0.15418$ nm), at a diffraction angle range of 2θ from 10 to 70° in reflection mode. The surface morphology was analyzed using scanning electron microscope (SEM) FEI IN SPECTS Company, Philips, Holland, environmental scanning without coating. Furthermore, transmission electron microscope (TEM) images of GO were taken with a JEOL JEM-2100 electron microscopy at an acceleration voltage of 120 kV. The thermal stability was carried out using a TGA Perkin-Elmer (STA6000), with a heating rate (10 °C/min). The temperature ranged from room temperature up to 800 °C under air atmosphere

(50 mL/min). The magnetic property of material can be characterized by studying its magnetization versus the magnetic field (M–H loop). This loop can be used as an indicator for the presence of an ordered magnetic structure using a vibrating sample magnetometer (VSM, Lakeshore 7410, USA) with a maximum applied a magnetic field of 20 kOe at room temperature. To reveal the point of zero charge (PZC) of the sorbent, zeta potentials (Zetasizer Nano S, Malvern Instruments, UK) at different pH (3–9) were measured.

Sorption Studies

Sorbents Comparative Study

A comparative adsorption study was estimated to identify the best efficient sorbent by adding the prepared sorbents to 100 ml of 100 mg/L Pb²⁺ solutions. The mixtures were shaken for (30, 60, and 120 min) then, the solutions were filtered and the remaining Pb²⁺ concentrations were determined by the atomic absorption spectrometer (Varian SpectraAA220). The removal efficiency (R%) was calculated using the following equation:

$$R\% = \left(C_o - \frac{C_t}{C_o} \right) \times 100 \quad (1)$$

where; C_o and C_t are the initial concentration and the remaining concentration of Pb²⁺ (mg/L) after contact time (t), respectively.

Effect of Contact Time on the Removal Efficiency

The batch experiments have been employed to study the influence of contact time on the removal efficiency by adding 0.15 g of EDTA/Si/mGO/AmCMC to 100 mL (1.5 g/L) of Pb²⁺ solutions (100 mg/L) and shacked at room temperature for a certain time (5–120 min). The regular procedure of filtration and analysis was next applied to calculate the removal efficiency (R%).

Effect of pH on the Removal Efficiency

The influence of different pH (3–9) on the removal efficiency (R%) was studied using 100 mg/L of Pb²⁺. The pH of the solutions was adjusted by NaOH and HCl. The solutions were filtered after a contact time of 120 min and the residual Pb²⁺ concentrations were measured.

Effect of Sorbent Dosage on the Removal Efficiency

The effect of sorbent dosage (0.05, 0.1, 0.15, 0.2, and 0.25 g) in the removal efficiency of Pb²⁺ at pH 5.3 for 120 min was

estimated. The R% was calculated from Eq. (1) and the amount of Pb²⁺ uptakes (q) by the sorbent was calculated as follows:

$$q = (C_o - C_t) \times \left(\frac{V}{M} \right) \quad (2)$$

where, C_o and C_t are the initial and the residual ions concentration after the time (t), respectively. V is the volume of solution (ml), and M is the sorbent mass (g).

Effect of Initial Pb²⁺ Concentrations on the Removal Efficiency

The removal study at different concentrations of Pb²⁺ (10, 25, 50, 100, and 200 mg/L) was also investigated at optimum conditions for contact time (120 min), R% and q were calculated.

Kinetic and Isotherm Studies

Four different kinetic models namely; pseudo-first-order [35], pseudo-second-order [36], intra-particle diffusion [37], and Elovich [38] were used to identify the sorption kinetics of Pb²⁺ from aqueous solution. Furthermore, Langmuir [39], Freundlich [40], Temkin [40], and the Dubinin–Radushkevich (D-R) [41] adsorption isotherms were applied to study how the adsorbate molecules interact with the sorbent particles. The equations and constants of the kinetic models and sorption isotherms were listed clearly in the Table 1.

Results and Discussion

Preparation and Characterization of Sorbents

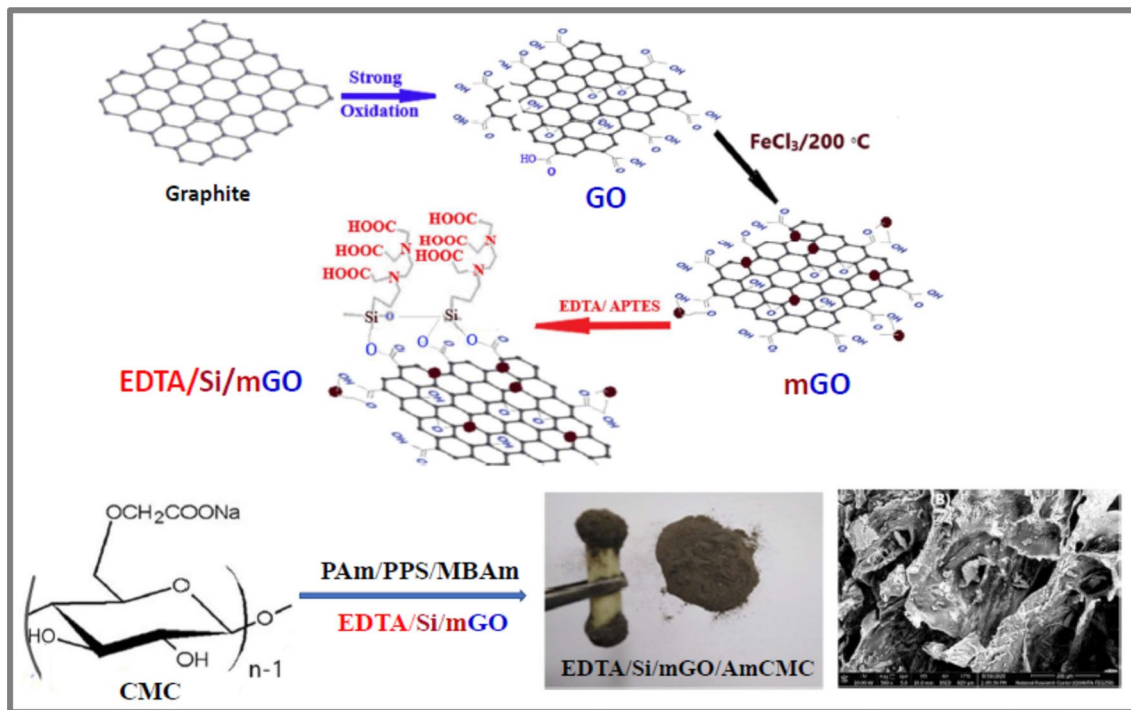
In this study, a crosslinked carboxymethyl cellulose grafted polyacrylamide (AmCMC) embedded with magnetic graphene oxide (mGO) and ethylene diamine tetra acetic acid as well as 3-aminopropyltriethoxysilane (EDTA/Si) was prepared as a sorbent (EDTA/Si/mGO/AmCMC) (Scheme 1). In the first, graphite was oxidized to GO by the Hummer method to introduce oxygenated functionalities such as carbonyl, carboxylic, and hydroxyl onto graphite layers, makes it hydrophilic and expand the layer separation.

The structure of the synthesized GO, as well as that of the parent graphite, was studied by XRD analysis. As shown in Fig. 1A, the XRD pattern of the graphite shows a sharp peak at $2\theta \sim 26^\circ$ and relatively weak intensity at $2\theta \sim 54^\circ$, corresponding to the (002) and (004) reflection planes of natural graphite, respectively. These peaks disappeared after oxidation and a new peak at $2\theta \sim 10^\circ$ due to (002) plane of GO appeared. The characteristic peak of GO at $2\theta \sim 11^\circ$ confirmed the successful chemical oxidation

Table 1 Kinetics and isotherms models for the sorption of Pb²⁺ onto sorbent

Variables	Variables	Variables	Variables
<i>Kinetics models</i>			
Pseudo-first-order	$\log (q_e - q_t) = \log q_e - \frac{k_1}{2.303} t$	q_e : equilibrium sorption capacity (mg/g) q_t : capacity of sorption (mg/g) at a time (t , min) k_1 : the rate constant (min^{-1})	$\log (q_e - q_t)$ Vs t
Pseudo-second-order	$\frac{t}{q_t} = \frac{1}{k_2 q_e} + \left(\frac{1}{q_e}\right) t$	k_2 : the rate constant (g/mg. min)	t/q_t Vs t
Intra-particle diffusion model	$q_t = k_p (t)^{0.5} + c$	k_p : intra-particle diffusion rate (mg. g ⁻¹ min ^{1/2}) C : constant	q_t Vs $t^{0.5}$
Elovich	$q_t = (1/\beta) \ln (\alpha\beta) + (1/\beta) \ln (t)$	β : the desorption constant (mg. g ⁻¹ .min) α : the initial adsorption rate (mg. g ⁻¹ .min ⁻¹)	q_t Vs $\ln t$
<i>Isotherms models</i>			
Langmuir isotherm ^a	$C_e/q_e = 1/bq_{max} + (1/q_{max}) C_e$ $R_L = \frac{1}{1+bC_0}$	b : the Langmuir constant (l/mg)	C_e/q_e Vs C_e
Freundlich isotherm ^b	$\ln q_e = \ln k_f + \left(\frac{1}{n}\right) \ln C_e$	q_{max} : the maximum sorption capacity (mg/g)	$\ln q_e$ Vs $\ln C_e$
Temkin isotherm	$q_e = (RT/b) \ln k_t + (RT/b) \ln C_e$	RL : separation factor	q_e Vs $\ln C_e$
(D–R) isotherm	$\ln q_e = \ln q_m - \beta \varepsilon^2$ $\varepsilon = RT \ln (1 + 1/C_e)$ $E = 1/(2\beta)^{0.5}$	k_f : the Freundlich constant	$\ln q_e$ Vs ε^2

^a $R_L = 1$: shows linear adsorption. $R_L = 0$: illustrates irreversible. $R_L > 1$: represents unfavorable adsorption. $0 < R_L < 1$: indicated good adsorption
^b $n = 1$: characterizes linear adsorption. $n < 1$: represents the chemical process. $n > 1$: designates the physical process



Scheme 1 A schematic representation of sorbent preparation

of graphite into GO and the formation of oxide groups. Consequently, increased the d-spacing and caused peak shift of graphite to a lower degree [42]. More confirmation

of graphite oxidation is the TEM image of GO (Fig. 1B) it was observed that the GO was formed by a layered structure due to the oxidation of the graphite. From the

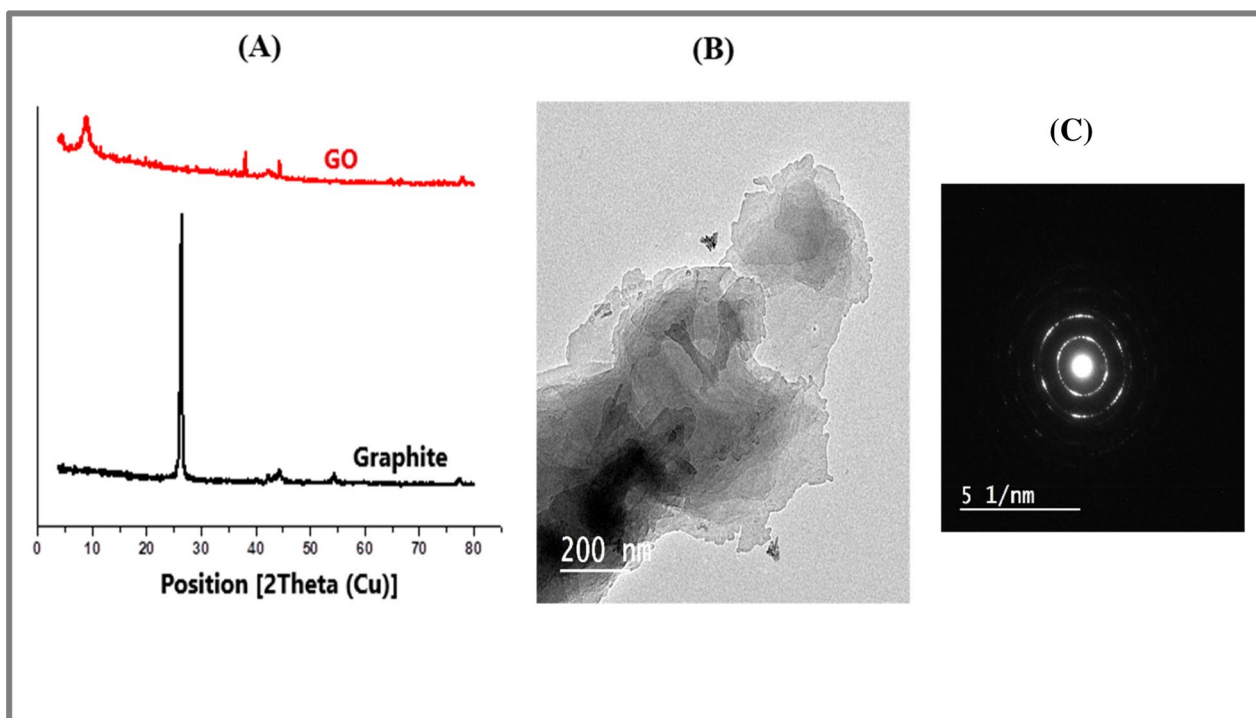


Fig. 1 X-ray diffraction patterns of graphite and graphene oxide (A), TEM image (B), and Electron diffraction pattern of GO (C)

electron diffraction pattern (Fig. 1C), GO particles have a typical diffuse ring with uniform sizes that have limited aggregation.

To increase the adsorption efficiency of GO and facilitate the separation of sorbent from the solution, the surface of GO was modified by environmentally functional groups that is magnetic nanoparticles followed by EDTA. The magnetite was loaded onto GO by solvothermal and new significant diffraction peaks appeared at $2\theta \sim 29, 35, 43, 53, 57,$ and 62° are matched well with the data from the JCPDS card (19–0629) for Fe_3O_4 which attributed to the crystal planes of Fe_3O_4 . However, the intensity of the diffraction peak of GO (at $2\theta \sim 10^\circ$) was decreased, which means that the loading of magnetite destroyed the layer stacking of GO sheets [43].

Since EDTA is a tetradentate ligand has two nitrogen atoms and two oxygen atoms in separate four carboxyl groups. It can act as scavenge-chelating agents which can capture metals through several powerful bonds. Accordingly, EDTA/Si/mGO was synthesized through a chemical reaction between the OH^- groups of hydroxyl and carboxyl on the surface of mGO and alkoxy groups of silanes. From X-ray diffraction (Fig. 2A) the peak of GO (at $2\theta \sim 10^\circ$) was not observed in EDTA/Si/mGO and no phase change of magnetite occurred through EDTA modification. The peak at $2\theta \sim 15^\circ$ and the broad peak at $2\theta \sim 23^\circ$ in EDTA/Si/mGO could be related to EDTA, suggesting that EDTA was well distributed on the mGO [44].

After loading of magnetite onto GO and modified with EDTA/Si giving EDTA/Si/mGO, the sorbent composite was prepared by loading the EDTA/Si/mGO onto polyacrylamide grafted CMC during the grafting process. The disappearance of most peaks of EDTA/Si/mGO on the X-ray diffraction of sorbent composite and appear new peaks at $2\theta \sim 17$ and 27° which could be related to acrylamide grafted CMC suggesting that EDTA/Si/mGO was well distributed on the polyacrylamide grafted CMC (Fig. 2A).

The anchoring of functional groups on the GO surface and their loading onto polyacrylamide grafted CMC was approved by FTIR spectra (Fig. 2B). From the IR spectra of CMC, it showed a broad absorption band at 3350 cm^{-1} , due to the stretching frequency of the $-\text{OH}$ group. The band at 2920 cm^{-1} and a strong absorption band at 1620 cm^{-1} were due to C–H stretching vibration and $-\text{COO}$ groups. The bands around 1420 and 1320 cm^{-1} were assigned to CH_2 scissoring and $-\text{OH}$ bending vibration, respectively while the band at 1100 cm^{-1} indicates the stretches of C–O group. By loading EDTA/Si/mGO onto AmCMC. The FTIR spectra of sorbent composites confirmed the well-distributed of EDTA/Si/mGO on the acrylamide grafted CMC is the decrease in band intensity of $-\text{OH}$ groups at 3350 cm^{-1} due to the weakening of hydrogen bonds among the $-\text{OH}$ groups. Furthermore, the peak at 1620 cm^{-1} was shifted to a higher wavenumber with the weakening of its intensity. Another remarked aspect is the disappearance of peak at

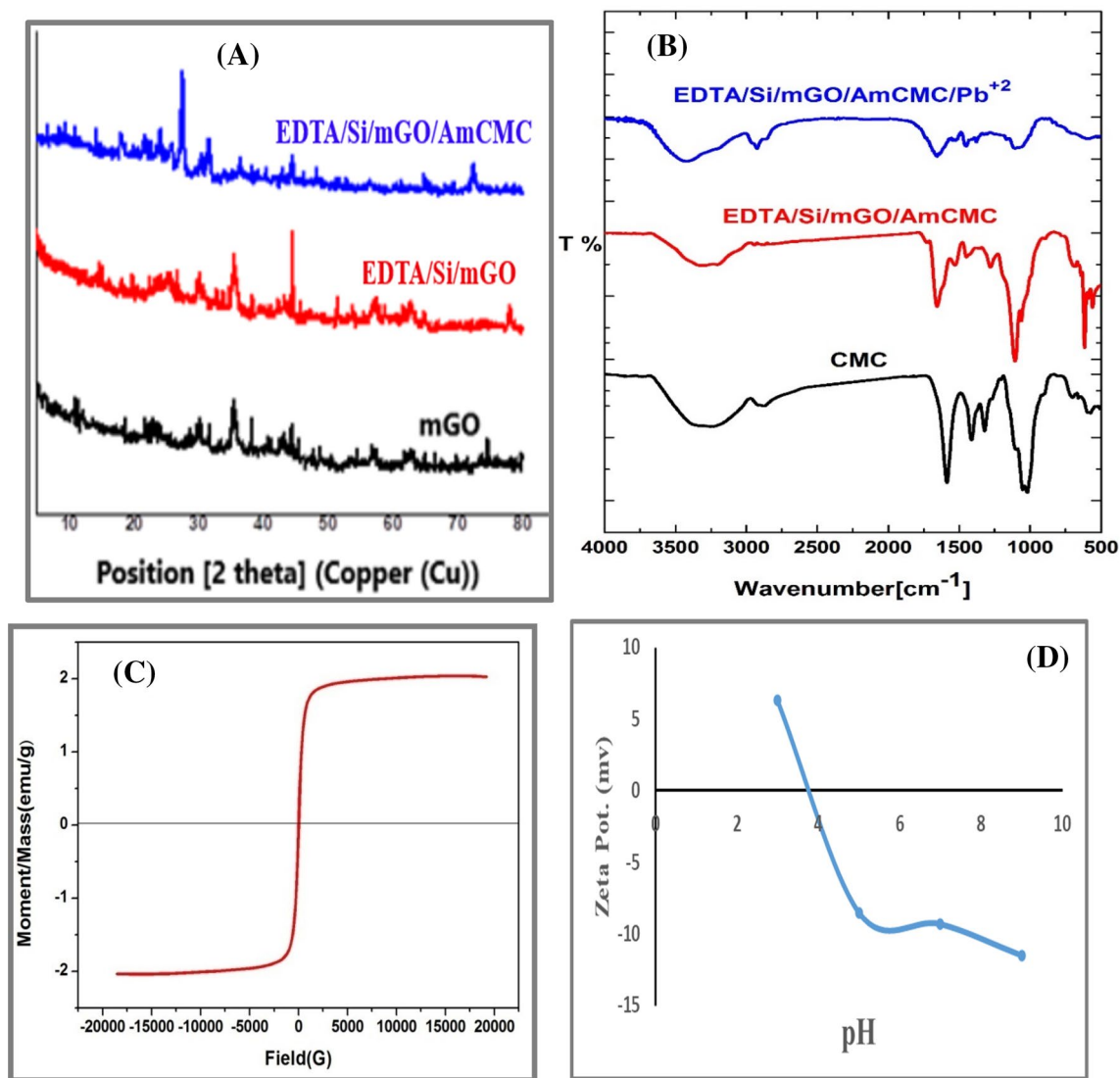


Fig. 2 XRD of mGO, EDAT/ Si/mGO, and EDTA/Si/mGO/AmCMC (A), FTIR spectra of CMC and EDTA/Si/mGO/AmCMC (B), Magnetization of EDTA/Si/mGO/AmCMC (C), and Zeta potential of EDTA/Si/mGO/AmCMC (D)

2920 cm⁻¹ and sorbents showed a characteristic absorption band around 580 cm⁻¹ that assigned to the stretching vibration frequency of the metal–oxygen (M–O) [45–47]. More confirmation is the appearance of chromatistic peaks of mGO with EDTA which are 1100, 1250, 1560, 1650, 1720, and 2923 cm⁻¹ characteristic to stretches of C–O in epoxy, hydroxyl, and carboxyl groups, C–OH stretching vibration, aromatic C=C, hydroxyl groups of alcohol and carboxyl of mGO, C–O stretching vibration of –COOH, and –CH bond stretching respectively [44]. The spectral analysis of sorbent after adsorption of Pb²⁺ showed that the peaks either decrease in intensity, shift, or disappear which justifies the feasibility of the adsorption process [48].

The magnetization at room temperature of the prepared composite was done by Vibrating Sample Magnetometer

(VSM), ± 20 kG, to examine the possibility for the development of their magnetic properties. Figure 2C shows that magnetization increased with the magnetic field until saturation with a saturation magnetization M_s = 2.039 emu/g. Also, it shows a symmetric hysteresis loop confirming the presence of ferromagnetic behavior with a soft magnetic order where the coercivity (H_c) is equal to 18.85 G. The saturated hysteresis loops for composite confirmed the presence of magnetic order released from the magnetic particles that loaded onto GO.

Figure 2D shows the zeta potential measurements of the EDTA/Si/mGO/AmCMC composite at pH 3–9. The data presented that the point of zero charge of the sorbent at pH 3.8. This means that at pH less than 3.8 the sorbent will be positively charged inhibiting the positively

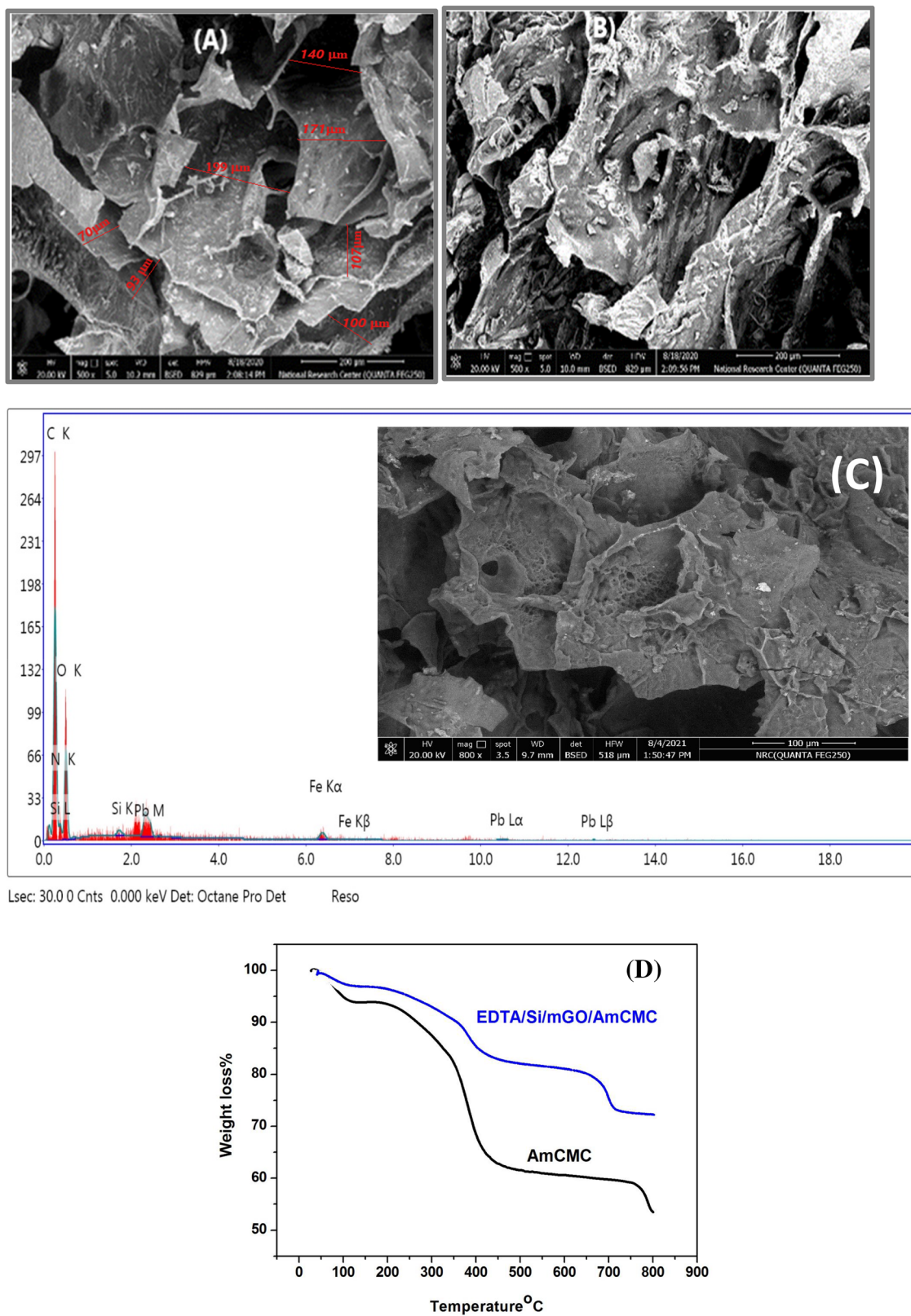


Fig. 3 SEM images of AmCMC (A), EDTA/Si/mGO/AmCMC (B), and (C) EDX of EDTA/Si/mGO/AmCMC after absorption (D) TGA curves of AmCMC and EDTA/Si/mGO/AmCMC sorbents

charged Pb^{2+} adsorption while at pH above the zero-charge point, it will carry a negative charge which promoting Pb^{2+} removal [49].

SEM micrographs for the AmCMC (Fig. 3A) and EDTA/Si/mGO loaded AmCMC (Fig. 3B) proved the incorporation of EDTA/Si/mGO in AmCMC and resulted in remarkable changes in the surface morphology of AmCMC. The AmCMC has an interconnected laminar structure with randomly distributed pores with an average diameter range of 125 μm . By loading EDTA/Si/mGO, the surface morphology revealed the formation of a layer and high distribution of EDTA/Si/mGO throughout the surface of AmCMC.

The immobilization of EDTA/Si/mGO onto the AmCMC will be affected its thermal stability. In order to evaluate this effect, TGA analysis of the AmCMC and EDTA/Si/mGO loaded AmCMC was performed (Fig. 3C).

The thermal degradation of AmCMC occurs in three steps, the initial step started at ~ 110 $^{\circ}\text{C}$ with $\sim 12\%$ weight loss due to dehydration. The second step was from 200 to 450 $^{\circ}\text{C}$ resulting in $\sim 78\%$ weight loss which could be ascribed to the decomposition of the crosslinked polymer chains. The third step started at 750–800 $^{\circ}\text{C}$ with $\sim 95\%$ weight loss due to the pyrolysis of the cellulose backbone [50]. As we expected the thermal stability has improved by loading the EDTA/Si/mGO onto AmCMC. The TGA curve of EDTA/Si/mGO/AmCMC demonstrated three degradation steps (Fig. 3C). The sample started breaking down around ~ 400 $^{\circ}\text{C}$ with $\sim 30\%$ weight loss then further degradation at ~ 660 $^{\circ}\text{C}$ with $\sim 40\%$ weight. The decomposition was resumed at ~ 775 $^{\circ}\text{C}$ losing $\sim 55\%$ of the original sample mass due to the pyrolysis of the cellulose backbone with residual ash $\sim 45\%$.

Sorption Study

Comparative Study on the Removal Efficiency

Figure 4A shows a comparative study on the removal efficiency of the prepared sorbents, AmCMC and EDTA/Si/mGO/AmCMC, for Pb^{2+} from aqueous solution after different times namely 30, 60, and 120 min. The data showed that EDTA/Si/mGO/AmCMC has the highest removal efficiency for Pb^{2+} over other AmCMC sorbent, which reached 86, 88, and 92% after 30, 60, and 120 min respectively. The higher removal efficiency of this sorbent can be attributed to the presence of EDTA/mGO system as Pb^{2+} can react with chelating groups such as $-\text{COOH}$, $-\text{NH}_2$, and $-\text{OH}$. Due to the high removal efficiency of EDTA/Si/mGO/AmCMC sorbent, the other adsorption conditions will be studied by this sorbent only.

Effect of Contact Time on the Removal Efficiency

Figure 4B displaying the effect of contact time on the removal efficiency of Pb^{2+} by the prepared sorbents such as EDTA/Si/mGO/AmCMC. It can be seen that a quick removal of Pb^{2+} within the first 5 min of the adsorption process was obtained. Next, a slower sorption step continued until reaching a state of equilibrium. This behavior is due to the availability of sufficient vacancies and cleaving groups such as $-\text{COOH}$, $-\text{NH}_2$, and $-\text{OH}$ in the initial of the reaction but after this contact time, active sites became occupied [51]. On the other side, the kinetic studies of adsorption of Pb^{2+} by sorbent were elucidated after applying the pseudo-first-order, pseudo-second-order, intra-particle diffusion model, and Elovich model. The kinetic model's constants and correlation coefficients of Pb^{2+} elaborate in Table 2. Interestingly from the data, the kinetics of the sorption reaction was perfectly fitted to the pseudo-second-order model (Fig. 4C) which assumes that the rate of solute sorption is directly proportional to the square of the number of vacant binding sites [52]. This due to the higher correlation coefficient value ($R^2 = 0.9992$), and the close matching between the experimental ($q_e = 58.67$ mg/g) and calculated ($q_e = 58.47$ mg/g) uptake from this model [4, 5].

Effect of pH on the Removal Efficiency

One of the most essential parameters which affect the removal efficiency of metal ions is pH value. Figure 5A revealing the removal efficiency of 100 mg/L Pb^{2+} by 0.15 g EDTA/Si/mGO/AmCMC cover the pH range of 3–9. The data clarified that as pH increase, the removal efficiency increase from 40 to 98%. At low pH values, less Pb^{2+} removal is observed which is attributed to the presence of a large number of protons (H^+) that may have adsorbed on the prepared sorbent sites rather than Pb^{2+} [53]. At high pH values, the H^+ competition disappears and sorbent carry a negative charge as previously reported in zeta potential measurements that increases attraction with Pb^{2+} thus increases the removal [49]. In alkaline media (pH higher than 8.0), it is known that precipitation plays a major role in removing metal ions which inhibits the adsorption process [9].

Effect of Sorbent Dosage on Removal Efficiency of Pb^{2+}

The sorbent dosage used in the sorption process is also important in the removal of metal ions from a solution. Figure 5B illustrates the effect of the sorbent dose from 0.05 to 0.25 g on the removal efficiency and the uptake capacity while maintaining other parameters fixed i.e., pH = 5.3, time = 120 min, and conc. = 100 mg/L. As expected, the removal efficiency of Pb^{2+} increased from 74 to 96% with increasing the amount

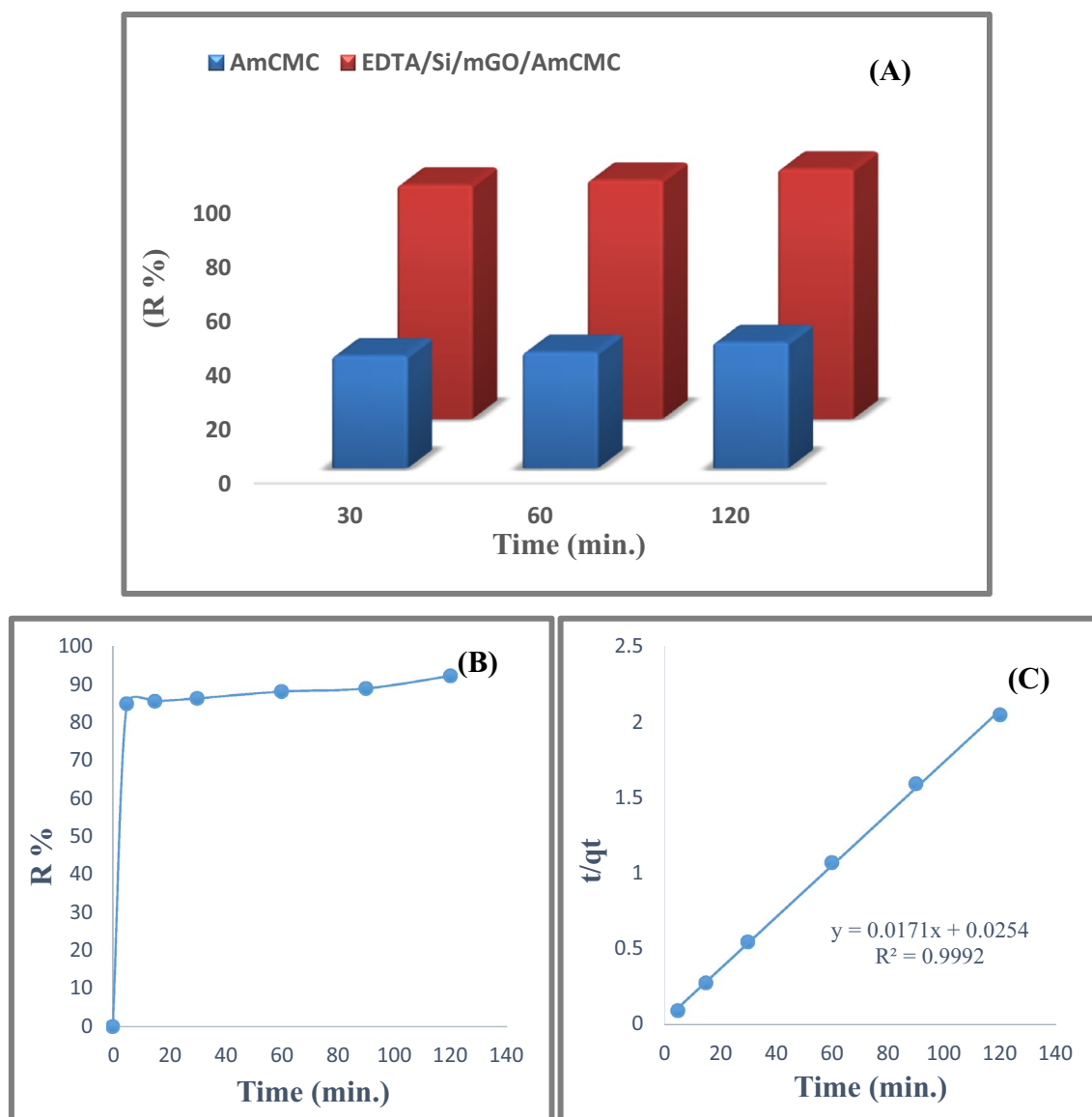


Fig. 4 A The removal efficiency of Pb²⁺ by the prepared sorbents for 30, 60, and 120 min as contact times and sorbents dosage was 0.15 g/100 mL, (B, C) the removal efficiency of 100 mg/L Pb²⁺, and

Pseudo-second-order adsorption fitting model for Pb²⁺ by 0.15 g of EDTA/Si/mGO/AmCMC respectively as a function of contact time

of the sorbent added which attributed to the increase of the active sites available for the Pb²⁺ removal [54]. Conversely, the removal efficiency of Pb²⁺ increased, the uptake capacity decreased from 140 to 36 mg/g with increasing the sorbent dosage due to the repulsion between the few Pb²⁺ occurring in the solution and the high-density volume of the already adsorbed metal ions [55, 56].

Effect of the Initial Pb²⁺ Concentrations on the Removal Efficiency

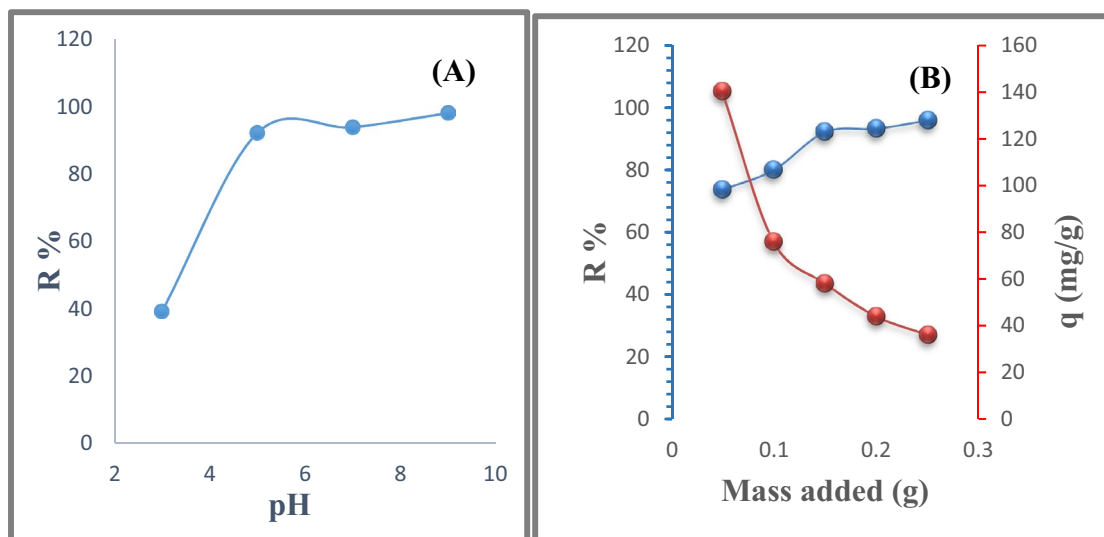
The Pb²⁺ concentration affects the adsorption process, so the removal efficiency by 0.15 g of sorbent was carried out

with different Pb²⁺ concentrations (Fig. 6A). The data show that as the initial concentration of Pb²⁺ increased from 10 to 200 mg/L, the removal efficiency decreased from 98 to 60% and this recognized the lacking sufficient active sites for adsorption [57]. On the contrary, the uptake capacity increase from 3 to 80 mg/g with increasing the concentration and this attributed to the ratio between Pb²⁺ and sorbent is sufficient to provide a driving force to overcome the mass transfer resistance between them [4, 5].

On the other hand, to illustrate how the Pb²⁺ interact with the sorbents; Langmuir, Freundlich, Temkin, and Dubinin–Radushkevich (D–R) isotherm models were studied. The constants and correlation coefficients calculated

Table 2 Constants of kinetics models and isotherms models for the removal of Pb^{2+} onto sorbent (EDTA/Si/mGO/AmCMC)

Constants of kinetics models				
Pseudo-first-order	K_1 (min^{-1})	$q_e(\text{exp.})$ (mg/g)	$q_e(\text{cal.})$ (mg/g)	R^2
	0.0096	58.67	4.9	0.993
Pseudo-second-order	K_2 (g/mg min)	$q_e(\text{exp.})$ (mg/g)	$q_e(\text{cal.})$ (mg/g)	R^2
	0.01	58.67	58.48	0.9992
Intra-particle diffusion model	K_p ($\text{mg} \cdot \text{g}^{-1} \cdot \text{min}^{1/2}$)	C		R^2
	0.489	52.53		0.914
Elovich	β ($\text{mg} \cdot \text{g}^{-1} \cdot \text{min}$)	α ($\text{mg} \cdot \text{g}^{-1} \cdot \text{min}^{-1}$)		R^2
	0.787	4.29×10^{17}		0.7899
Constants of isotherms models				
Langmuir isotherm	q_{max} (mg/g)	b (L/mg)		R^2
	86.2	0.155		0.995
Freundlich isotherm	n	K_f		R^2
	1.95	11.17		0.969
Temkin isotherm	k_t (mol/L)	B		R^2
	4.99	12.2		0.9124
(D–R) isotherm	q_{max} (mg/g)	β	E (kJ/mol)	R^2
	32.1	6×10^{-7}	2.67	0.6429

**Fig. 5** **A** Effect of the pH of the solution on the removal efficiency of Pb^{2+} by 0.15 g of EDTA/Si/mGO/AmCMC sorbent after contact time 120 min. **B** Effect of the sorbent dosage on the removal efficiency of Pb^{2+} and uptake capacity of sorbent after contact time 120 min

from the isotherm models were listed in Table 2. Remarkably from the data (Fig. 6B), the sorption of Pb^{2+} was fitted to the Langmuir model due to the higher correlation coefficient ($R^2 = 0.995$) value which assumes monolayer adsorption of the Pb^{2+} onto active sites of the sorbent's surface [58]. The value of $n > 1$ in Freundlich and $E < 8$ in (D–R) model demonstrating that the adsorption is a physical process [40]. Moreover, the separation factor (R_L) values were found to be

in the range from 0 to 1, which proposing favorable adsorption between Pb^{2+} and EDTA/Si/mGO/AmCMC.

The maximum Pb^{2+} sorption capacities (q_{max}) of the sorbent (EDTA/Si/mGO/AmCMC) which calculated from the Langmuir model were compared with different sorbents in previous studies (Table 3). The data indicated that the prepared sorbent has a good ability for the removal of Pb^{2+} from an aqueous solution.

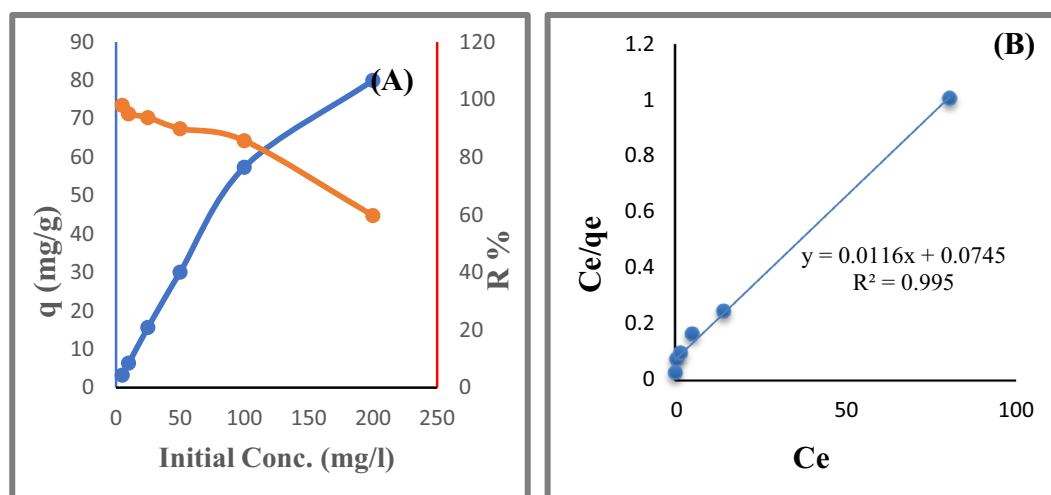


Fig. 6 **A** Effect of the initial Pb^{2+} concentrations on the removal efficiency and the uptake, **B** The Langmuir adsorption fitting isotherm at (sorbents dose = 0.15 g and contact time = 120 min.)

Table 3 Comparison of adsorption capacities for Pb^{2+} with different sorbents

Sorbents	Adsorption capacity(mg/g)	Reference
Callinectes sapidus biomass	31.44	[55, 56]
Cellulose-MT-CBM bio sorbents	39.02	[59]
Cellulose	43.96	[60]
Ak powder/ Fe_3O_4 magnetic composite	54.94	[61]
Red mud	64.79	[62]
Natural clinoptilolite	80.93	[63]
EDTA/Si/mGO/AmCMC	86.00	Present work

Conclusion

An excellent eco-friendly sorbent was successfully prepared by the introduction of EDTA groups to the mGO surface through a salinization process followed by embedded onto AmCMC for Pb^{2+} removal from aqueous solution. The adsorption was studied by studying the effect of contact time, pH, sorbent dosage of sorbent, and concentrations of Pb^{2+} on removing efficiency of the prepared sorbent. The results illustrated that the removal efficiency of Pb^{2+} by EDTA/Si/mGO/AmCMC (92%) is higher than that of AmCMC (46%) after a contact time of 120 min. A great increase in the removal efficiency was detected with increasing contact time, pH, and sorbent dosage, while a significant decrease was observed with increasing the initial concentration of Pb^{2+} . The higher correlation

coefficient ($R^2 = 0.9992$) indicated that the kinetics of the sorption reaction could be fitted to a pseudo-second-order model. Furthermore, the isothermal results indicate that the Langmuir isotherm was a much better model due to the higher correlation coefficient ($R^2 = 0.995$) and a maximum adsorption capacity for EDTA/Si/mGO/AmCMC of 86 mg/g was obtained.

Acknowledgements The authors acknowledge the Academy of Scientific Research and Technology (ASRT), Egypt (Grant ASRT-19-06), for financial support of the bilateral research activities.

Author Contributions Study conception and design: SD and KHK, Acquisition of data: SD and KHK. Analysis and interpretation of data: SK. Drafting of the manuscript: SD, KHK, and SK. Critical revision: SK. All authors approved the final version to be submitted.

Funding This work was supported by the Academy of Scientific Research and Technology (ASRT), Egypt (Grant ASRT-19-06).

Data Availability All relevant data are within the manuscript and available from the corresponding author upon request.

Declarations

Conflict of interest All the authors hereby declare that they do not have any conflict of interest about this manuscript.

Consent to Participate All authors have participated in this work.

Consent to Publish All authors agree to publish.

Research Involving Human and Animal Participants This article does not contain any studies with human participants or animals performed by any of the authors.

References

- Li R et al (2018) Hybrid hydrogel with high water vapor harvesting capacity for deployable solar-driven atmospheric water generator. *Environ Sci Technol* 52(19):11367–11377
- Zhao F et al (2019) Super moisture-absorbent gels for all-weather atmospheric water harvesting. *Adv Mater* 31(10):1806446
- Haggag S et al (2020) Innovative synthesis of modified cellulose derivative as a uranium adsorbent from carbonate solutions of radioactive deposits. *Cellulose* 27:7093–7108
- Kamal K et al (2019) Methylene blue removal from wastewater using silica/corn cob nanocomposite. *Int J Dev* 8(1):81–93
- Kamal KH et al (2019) Adsorption of Fe ions by modified carrageenan beads with tricarboxy cellulose: kinetics study and four isotherm models. *Desalin Water Treat* 165:281–289
- Yang L et al (2020) Energy harvesting from atmospheric humidity by a hydrogel-integrated ferroelectric-semiconductor system. *Joule* 4(1):176–188
- Sardar K et al (2013) Heavy metals contamination and what are the impacts on living organisms. *Greener J Environ Manage Public Safety* 2(4):172–179
- Abou-Zeid RE et al (2020) Grafted TEMPO-oxidized cellulose nanofiber embedded with modified magnetite for effective adsorption of lead ions. *Int J Biol Macromol* 167:1091
- Mohammad AM et al (2017) Efficient treatment of lead-containing wastewater by hydroxyapatite/chitosan nanostructures. *Arab J Chem* 10(5):683–690
- Rengaraj S et al (2002) Studies on adsorptive removal of Co (II), Cr (III) and Ni (II) by IRN77 cation-exchange resin. *J Hazard Mater* 92(2):185–198
- Cai G-B et al (2010) Synthesis of polyacrylic acid stabilized amorphous calcium carbonate nanoparticles and their application for removal of toxic heavy metal ions in water. *J Phys Chem* 114(30):12948–12954
- Fu F et al (2007) Effective removal of coordinated copper from wastewater using a new dithiocarbamate-type supramolecular heavy metal precipitant. *Chemosphere* 69(11):1783–1789
- Rao MM et al (2009) Removal of some metal ions by activated carbon prepared from *Phaseolus aureus* hulls. *J Hazard Mater* 166(2–3):1006–1013
- Solanki P et al (2010) Synthesis of zeolite from fly ash and removal of heavy metal ions from newly synthesized zeolite. *E-J Chem* 7(4):1200–1205
- Frimpong RA et al (2007) Synthesis and temperature response analysis of magnetic-hydrogel nanocomposites. *J Biomed Mater Res Part A* 80(1):1–6
- Kabir A et al (2018) Water recycling efficacies of extremely hygroscopic, antifouling hydrogels. *RSC Adv* 8(66):38100–38107
- Abou-Yousef H et al (2021) Biocompatible hydrogel based on aldehyde-functionalized cellulose and chitosan for potential control drug release. *Sustain Chem Pharm* 21:100419
- Pashaei-Fakhri S et al (2021) Crystal violet dye sorption over acrylamide/graphene oxide bonded sodium alginate nanocomposite hydrogel. *Chemosphere* 270:129419
- Peighambaroust SJ et al (2020) Removal of malachite green using carboxymethyl cellulose-g-polyacrylamide/montmorillonite nanocomposite hydrogel. *Int J Biol Macromol* 159:1122–1131
- Abou-Zeid RE et al (2018) Novel method of preparation of tricarboxylic cellulose nanofiber for efficient removal of heavy metal ions from aqueous solution. *Int J Biol Macromol* 119:207–214
- Sirviö J et al (2011) Dialdehyde cellulose microfibers generated from wood pulp by milling-induced periodate oxidation. *Carbohydr Polym* 86(1):260–265
- Akl EM et al (2020) Preparation and characterization of novel antibacterial blended films based on modified carboxymethyl cellulose/phenolic compounds. *Polym Bull* 78:1–25
- Khattab TA et al (2019) Smart microfibrillated cellulose as swab sponge-like aerogel for real-time colorimetric naked-eye sweat monitoring. *Talanta* 205:120166
- Dacrory S et al (2018) Preparation and characterization of eco-friendly carboxymethyl cellulose antimicrobial nanocomposite hydrogels. *J Renew Mater* 6(5):536–547
- Mohammadi R et al (2021) Carboxymethylcellulose/polyacrylic acid/starch-modified Fe₃O₄ interpenetrating magnetic nanocomposite hydrogel beads as pH-sensitive carrier for oral anticancer drug delivery system. *Eur Polym J* 153:110500
- Mekheimer RA et al (2011) Simple, three-component, highly efficient green synthesis of thiazolo [3, 2-a] pyridine derivatives under neat conditions. *Synth Commun* 41(17):2511–2516
- Madarang CJ et al (2012) Adsorption behavior of EDTA-graphene oxide for Pb (II) removal. *ACS Appl Mater Interfaces* 4(3):1186–1193
- Dacrory S et al (2021) Cyanoethyl cellulose/BaTiO₃/GO flexible films with electroconductive properties. *ECS J Solid State Sci Technol*. <https://doi.org/10.1149/2162-8777/ac1c56>
- Ghanem AF et al (2020) Synergistic effect of zinc oxide nanorods on the photocatalytic performance and the biological activity of graphene nano sheets. *Heliyon* 6(2):e03283
- Foroutan R et al (2021) Adsorption mercury, cobalt, and nickel with a reclaimable and magnetic composite of hydroxyapatite/Fe₃O₄/polydopamine. *J Environ Chem Eng* 9(4):105709
- Peighambaroust SJ et al (2021) Decoration of Citrus limon wood carbon with Fe₃O₄ to enhanced Cd²⁺ removal: a reclaimable and magnetic nanocomposite. *Chemosphere* 2021:131088
- Magdalena A et al (2018) EDTA-functionalized Fe₃O₄ nanoparticles. *J Phys Chem Solids* 113:5–10
- Sahoo, J. K., et al. (2017). EDTA functionalized magnetic nanoparticle as a multifunctional adsorbent for Congo red dye from contaminated water. *AIP Conference Proceedings*, AIP Publishing LLC
- Dacrory S (2021) Antimicrobial activity, DFT Calculations, and molecular docking of dialdehyde cellulose/graphene oxide film against Covid-19. *J Polym Environ* 29:2248
- Sharma N, Nandi BK (2013) Utilization of sugarcane bagasse, an agricultural waste to remove malachite green dye from aqueous solutions. *J Mater Environ Sci* 4(6):1052–1065
- Azizian SJJOC, Science I (2004) Kinetic models of sorption: a theoretical analysis. *J Colloid Interface Sci* 276(1):47–52
- Doğan M et al (2004) Kinetics and mechanism of removal of methylene blue by adsorption onto perlite. *J Hazard Mater* 109(1–3):141–148
- Bharathi K, Ramesh SJAWS (2013) Removal of dyes using agricultural waste as low-cost adsorbents: a review. *Appl Water Sci* 3(4):773–790
- Gupta S, Babu BV (2009) Removal of toxic metal Cr (VI) from aqueous solutions using sawdust as adsorbent: equilibrium, kinetics and regeneration studies. *Chem Eng J* 150(2–3):352–365
- Senthil Kumar P et al (2014) Adsorption of basic dye onto raw and surface-modified agricultural waste. *Environ Prog Sustain Energy* 33(1):87–98
- Dubin M (1947) The equation of the characteristic curve of activated charcoal. *Dokl Akad Nauk SSSR* 55:327
- Jiao X et al (2017) Comparison of the characteristic properties of reduced graphene oxides synthesized from natural graphites with different graphitization degrees. *RSC Adv* 7(82):52337–52344
- Kamel S et al (2020) Carboxymethyl cellulose-hydrogel embedded with modified magnetite nanoparticles and porous carbon: effective environmental adsorbent. *Carbohydr Polym* 242:116402

44. Marnani NN, Shahbazi A (2019) A novel environmental-friendly nanobiocomposite synthesis by EDTA and chitosan functionalized magnetic graphene oxide for high removal of Rhodamine B: adsorption mechanism and separation property. *Chemosphere* 218:715–725
45. Abou Hammad A et al (2019) A novel electromagnetic biodegradable nanocomposite based on cellulose, polyaniline, and cobalt ferrite nanoparticles. *Carbohydr Polym* 216:54–62
46. Dacrory S et al (2019) Functionalization and cross-linking of carboxymethyl cellulose in aqueous media. *Cellul Chem Technol* 53(1–2):23–33
47. Dacrory S et al (2020) In situ synthesis of Fe₃O₄@ cyanoethyl cellulose composite as antimicrobial and semiconducting film. *Carbohydr Polym* 2020:116032
48. Foroutan R et al (2021) Hydroxyapatite biomaterial production from chicken (femur and beak) and fishbone waste through a chemical less method for Cd²⁺ removal from shipbuilding wastewater. *J Hazard Mater* 413:125428
49. Salah TA et al (2014) Development of nano-hydroxyapatite/chitosan composite for cadmium ions removal in wastewater treatment. *J Taiwan Inst Chem Eng* 45(4):1571–1577
50. El-Sayed NS et al (2019) Development of electrical conducting nanocomposite based on carboxymethyl cellulose hydrogel/silver nanoparticles@ polypyrrole. *Synth Metals* 250:104–114
51. Abd El-Aziz M et al (2018) Biodegradable grafting cellulose/clay composites for metal ions removal. *Int J Biol Macromol* 118:2256–2264
52. Choudhary B, Paul D (2018) Isotherms, kinetics and thermodynamics of hexavalent chromium removal using biochar. *J Environ Chem Eng* 6(2):2335–2343
53. Boushehrian MM et al (2020) Ultrasonic assisted synthesis of Kaolin/CuFe₂O₄ nanocomposite for removing cationic dyes from aqueous media. *J Environ Chem Eng* 8(4):103869
54. Nasuha N et al (2010) Rejected tea as a potential low-cost adsorbent for the removal of methylene blue. *J Hazard Mater* 175(1–3):126–132
55. Foroutan R et al (2019) Eggshell nano-particle potential for methyl violet and mercury ion removal: Surface study and field application. *Adv Powder Technol* 30(10):2188–2199
56. Foroutan R et al (2019) Characteristics and performance of Cd, Ni, and Pb bio-adsorption using *Callinectes sapidus* biomass: real wastewater treatment. *Environ Sci Pollut Res* 26(7):6336–6347
57. Aksu Z, Tezer SJPB (2005) Biosorption of reactive dyes on the green alga *Chlorella vulgaris*. *Process Biochem* 40(3–4):1347–1361
58. Langmuir I (1916) The constitution and fundamental properties of solids and liquids. Part I. Solids. *J Am Chem Soc* 38(11):2221–2295
59. Mwandira W et al (2020) Cellulose-metallothionein biosorbent for removal of Pb (II) and Zn (II) from polluted water. *Chemosphere* 246:125733
60. Aquino R et al (2018) Adsorptive removal of lead (Pb 2) ion from water using cellulose acetate/polycaprolactone reinforced nanostructured membrane. *IOP Conf Ser* 191(1):012139
61. Shafiee M et al (2019) Application of oak powder/Fe₃O₄ magnetic composite in toxic metals removal from aqueous solutions. *Adv Powder Technol* 30(3):544–554
62. Gupta VK et al (2001) Process development for the removal of lead and chromium from aqueous solutions using red mud—an aluminium industry waste. *Water Res* 35(5):1125–1134
63. Günay A et al (2007) Lead removal from aqueous solution by natural and pretreated clinoptilolite: adsorption equilibrium and kinetics. *J Hazard Mater* 146(1–2):362–371

Publisher's Note Springer Nature remains neutral with regard to jurisdictional claims in published maps and institutional affiliations.

Authors and Affiliations

Sawsan Dacrory¹ · Kholod H. Kamal²  · Samir Kamel¹

✉ Kholod H. Kamal
kholod.hamdy@yahoo.com

¹ Cellulose and Paper Department, National Research Centre, 33 El Bohouth St, Dokki 12622, Egypt

² Water Pollution Research Department, National Research Centre, 33 El Bohouth St, Dokki 12622, Egypt